Reconstruction of Clinical dPET Data using Empirical Mode Decomposition Temporal Regularisation

Andrew McLennan[a], Sir Michael Brady[a] and Matt Kelly[b*]

[a]University of Oxford, UK
[b]Siemens Molecular Imaging, UK

Abstract. The current commercial practice of independently reconstructing temporally contiguous dynamic PET images ignores the temporal consistency between frames. We present a method which imposes a regularisation constraint based on the Empirical Mode Decomposition (EMD) iterative algorithm of Rilling. We apply the decomposition to full spatio-temporal volumes and use it for the reconstruction of dynamic PET data.
Instead of applying conventional wavelet-based thresholding to the Intrinsic Mode Functions (IMFs), we introduce locally defined and empirically-determined thresholding techniques. We show that EMD-based regularisation has the potential to produce superior quantitative reconstructions and examine the effect various thresholding methods have on the overall images.
We illustrate EMD-based spatio-temporal regularised reconstructions in simulated and clinical experiments. Our method outperforms conventional methods both in terms of SNR and Mean Square Error (MSE), and removes the need to temporally post-smooth the reconstruction.

1 Introduction

PET is a medical imaging modality which is able to record pharmacokinetic information. When a radiotracer such as ^{18}F-FDG is administered, the reconstruction of detected data enables the tracer's distribution to be visualised in-vivo. Dynamic PET typically involves detecting, and independently reconstructing, a contiguous sequence of scans ("frames"), which may range in duration from a few seconds to many minutes. The choice of frame durations is difficult to justify: short frames have higher temporal resolution but fewer counts, hence poorer SNR; long frames have higher spatial resolution and tend to increase SNR as well. Most clinical PET scans are static; we show the potential improvements in image quality possible when the goal of dynamic imaging is explicitly incorporated into the reconstruction algorithm. The main motivation of dynamic over static PET is that abnormal physiology provides clinicians with far more information than abnormal anatomy. This is especially true for cancer radiotherapy treatment plans, where there is growing evidence that PET is able to visualise a patient's response to treatment before anatomical changes are apparent. Detecting early response to treatment enables clinicians to modify the plan as required, reducing the patient's discomfort and improving their overall chance of survival.

Signal recovery from noisy estimates is a classic signal analysis problem. Many attempts have been made to reduce the noise inherent in dynamic PET using regularisation techniques. One idea is to apply Gaussian temporal filtering to smooth the Time Activity Curve (TAC) estimates [1]. Another is the method of Nichols et al, which estimates TACs using B-Spline temporal basis functions [2]. Reader et al. proposed using a specific compartmental model [3]. Kamasak et al. [4] extended the idea of Carson and Lange [5] of directly estimating kinetic parameters from the projection data, but requires that that compartmental model is known a priori. Various data-driven reconstruction methods have also been previously explored in the literature, such as PCA [6] and the KL transform [7]. Wavelet denoising has also been explored: there have been many attempts to remove noise from both the projection data as well as the reconstructed images. Shidhara et al. provides a good summary of some of these methods with emphasis on how their application effects pharmacokinetic parameter estimates [8]. Lee et al. [9] utilises Robust Wavelet Shrinkage and Verhaeghe et al. recently proposed a reconstruction algorithm using E-Spline wavelet-like temporal basis functions [10].

We explicitly incorporate a temporal regularisation procedure directly into the reconstruction algorithm. The method decomposes the spatio-temporal activity estimate into Intrinsic Mode Functions (IMF) and empirically regularises the reconstruction. The Empirical Mode Decomposition (EMD) iterative algorithm is used since it is both data-driven and multi-resolution. Our method results in improved dynamic PET reconstructions when tested on realistic simulated data and yields less noisy, visually enhanced images for clinical colorectal data.

*andrew.mclennan@new.ox.ac.uk; jmb@robots.ox.ac.uk; matthew.kelly@siemens.com

2 Method

2.1 Image Reconstruction

The forward projection model of dynamic PET for a matrix of F temporal I-dimensional detected projection data vectors $\mathbf{Y} \sim \text{Poisson}\left\{\hat{\mathbf{Y}}\right\}$ can be written as: $\hat{\mathbf{Y}} = \mathbf{PX} + \mathbf{R} + \mathbf{S}$; where $\mathbf{X}$ is the $J \times F$ spatio-temporal image activity matrix used to represent the dynamic radioactivity distributions; $\mathbf{P}$ is the forward projection matrix representing the probability that an emission from the j^{th} spatial basis function is detected by the i^{th} Line of Response (LOR); and $\mathbf{R}$ and $\mathbf{S}$ are the Randoms and Scatter contribution vectors to the expected data.

Substituting the forward projection model into the Log-Likelihood function of a Poisson process, differentiating, and then rearranging gives the conventional ML-EM algorithm [11] for reconstructing the spatio-temporal tracer distribution $\mathbf{X}$. We modify the conventional algorithm to include temporal regularisation to reduce noise. After each update of the F images using the ML-EM algorithm, the reconstruction volume is decomposed, denoised and then recomposed using the multi-resolution EMD transform. The overall algorithm for the combined multi-resolution regularisation and image reconstruction can be written as:

$$\mathbf{X}^{k+1}(t) = \frac{\tilde{\mathbf{X}}^{k}(t)}{\mathbf{P}^T\mathbf{1}}\mathbf{P}^T\frac{\mathbf{Y}(t)}{\mathbf{P}\tilde{\mathbf{X}}^{k}(t) + \mathbf{R}(t) + \mathbf{S}(t)} \tag{1}$$

$$\tilde{\mathbf{X}}^{k+1}(t) = \Psi\left(\Phi\left(\Psi^{-1}\left(\mathbf{X}^{k+1}(t)\right)\right)\right). \tag{2}$$

where the product and division of vectors are understood to be carried out element-wise (as in [3]), $\mathbf{1}$ represents a vector of $1's$, $\mathbf{X}^k$ is the current reconstruction estimate for all time frames obtained from Equation (1), $\tilde{\Psi}^{-1}$ and $\tilde{\Psi}$ are the forward and reverse EMD operators which perform the multi-resolution decomposition and recomposition, and Φ is the denoising operator. This alternating reconstruction-denoising procedure is an extension of the Silverman et al. [12] "Estimate-Maximise-Smooth" method to temporal data.

2.2 Empirical Mode Decomposition (EMD) Regularisation

EMD, also known as the Hilbert-Huang Transform [13], is a data-driven multicomponent signal analysis tool. It has similarities with the Wavelet Transform [14]; but rather than fixing the decomposition basis to a single pre-defined "mother" wavelet, it enables the transform to adaptively determine a variable set of Intrinsic Mode Function (IMF) frequency modes. Figure 1(a) shows an example EMD decomposition. Although it remains a heuristic method, each IMF is similar to a simple harmonic function; but far more general allowing both amplitude and frequency to vary with time.

As dynamic PET TACs consist of a smooth true signal component corrupted by noise, the individual IMFs can extract the non-true high-frequency signal components with varying amplitude and frequencies from the underlying true activity curve. For our application, we can decompose the k^{th} TAC estimate of voxel j into a series of C IMFs and a non-zero mean low-order polynomial residual term R using the EMD algorithm:

$$X_j^k = R_j + \sum_{c=1}^{C} \text{IMF}_\text{c}. \tag{3}$$

As high frequency signal components are contained in the initial IMFs, one can apply wavelet-based high frequency noise removal. Thresholding, or removing whole IMFs before recombination, enables the fully data-driven denoising process without user bias. Various EMD noise removal operators have been proposed in the literature [15, 16].

To denoise a signal using the EMD transform, we apply an operator Φ to the IMFs. We compare the result of traditional reconstruction methods with two EMD-based reconstruction methods. The first reconstructs TACs from those IMFs which have higher order than the minimal energy IMF $\tilde{c}$ [17]:

$$CMSE(\tilde{X}_c, \tilde{X}_{c+1}) = \frac{1}{N}\sum_{i=1}^{N}\left(\tilde{X}_c(t_i) - \tilde{X}_{c+1}(t_i)\right)^2 = \frac{1}{N}\sum_{i=1}^{N}\left(\text{IMF}_\text{c}(\text{t}_\text{i})\right)^2 \tag{4}$$

where X_c and X_{c+1} denote signals that are reconstructed starting from IMFs indexed by c and c+1 respectively. Thus, by calculating the energy of the various IMFs it is possible to determine which contain signal and which are dominated by noise.

The second method thresholds the IMF coefficients [18]. The threshold selection is non-trivial, however, especially in the case where noise is non-Gaussian and non-stationary. The method we use is to scale the traditional level specific Hard Thresholding value with the residual term in order to make the threshold non-stationary:

$$\tilde{\sigma}_c(t) = \hat{\sigma}_c * \mathrm{Residual(t)}, \quad (5)$$

$$\hat{\sigma}_c = \frac{\mathrm{median}\left(|\mathrm{IMF_c(t)}|\right)}{0.6745}. \quad (6)$$

3 Results and Discussion

Our EMD denoising algorithm was assessed using both highly realistic 3D+t PET-SORTEO simulation data and clinical colorectal data. The conventional static PET reconstruction algorithms: FBP, FBP Post-GS, OSEM, and OSEM with inter-iteration GS algorithms were applied as a means of comparing the performance of the proposed approaches. GS denotes the convolution of the current estimate with a temporal Gaussian kernel of size $\sigma = 1$. The quantitative accuracy of the reconstructions are compared by using the Mean Square Error (MSE) and Temporal Signal to Noise Ratio (TSNR) measures taken from Verhaeghe et al [10], and a Bias Vs. Noise measure taken from [19].

3.1 Simulated 1D TACs

Seven different TACs (Left & Right Ventricle taken from [10] and 1 compartment models taken from [19]) were compared to determine the effect of our methods on MSE and SNR. Each TAC was used to generate 100 noisy realisations by adding normally distributed noise proportional to the activity/frame duration at each temporal point.

Table 1(b) shows the results for one of the TACs (all other TACs give similar results). Bold numbers indicate which methods produced the better results. The Hard and Soft Thresholding methods are taken from [18]. We see that the two EMD-based regularisation schemes, New method and CMSE method, yield the best overall results on average. Also, the EMD methods are capable of extremely accurate estimates on some occasions and more investigation is needed to achieve these levels of result consistently. Finally, the largest MSE results are also lower for the EMD method indicating that GS in some case produces significantly worse estimates than EMD. Since EMD methods are data-driven, no user defined smoothing term is required, unlike Gaussian smoothing where a kernel needs to be selected. We note that even though the Residual provides a good TAC estimate, additional IMFs are required in order to accurately fit initial dynamics.

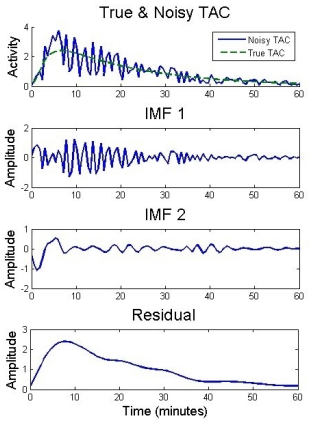

(a) Example IMF Decomposition

	SNR			MSE		
	Mean	Max	Min	Mean	Max	Min
None	10.75	12.23	9.09	0.0851	0.123	0.0597
GS	16.20	20.33	13.63	0.0247	0.043	0.0093
CMSE	**19.69**	**29.42**	**15.34**	**0.0132**	**0.040**	**0.0011**
Hard	15.28	25.64	1.60	0.0987	0.692	0.0027
Soft	14.08	24.30	1.03	0.1391	0.790	0.0037
New	**19.00**	**29.31**	**15.50**	**0.0139**	**0.028**	**0.0012**
Residual	4.05	20.99	0.96	0.490	0.802	0.0080

(b) Table of Results for an example biologically plausible TAC.

Figure 1. Example EMD frequency modes and results for 1D analysis

3.2 PET-SORTEO Simulated 3D+t PET Data

The PET-SORTEO Monte Carlo-based simulator [20] generated realistic dPET data. Biologically plausible TACs taken from [3] were assigned to the nine region 17.5cm diameter by 20cm long 3D+t phantom shown in Figure 2. TAC 1 was assigned to corner ROIs, TAC 2 to the middle ROI, TAC 3 to the remaining ROIs and TAC4 to the background. Thirty 120 second temporal frames produced sinograms of size $144 \times 288 \times 239$ covering a 1 hour scan acquisition. A total of approximately 1.1 million events were recorded along the central slice through the phantom for which we show results. Randoms and Scatter events were not included in this simulation as, in the ideal case, they would be perfectly

accounted for by the Randoms and Scatter matrices R and S respectively. Attenuation was also not simulated because it is assumed that this would be accounted for in practice using one of a variety of correction techniques. Images of size 128×128, for 10 iterations (8 subsets), were produced for reconstruction algorithms.

Figure 2 shows reconstruction slices for temporal frame 6. The results indicate that the new method produces better quality reconstructions than the conventional independent frame methods. This visual assessment is confirmed by Figure 3 which shows that the mean bias and mean noise of the new reconstruction method is generally lower than the conventional OSEM method for the different ROIs. Figure 3(a) shows results for the three activity regions for different levels of post-reconstruction spatial smoothing. Figure 3(b) shows results for different levels of post-reconstruction temporal smoothing (with voxel and overlapping spatial (SPS) basis functions). As the temporal smoothing for the new method only results in modifying the bias of the reconstruction (due to the smooth results produced by the EMD transform) as seen by the displacements along the horizontal axis, only spatial smoothing should be implemented post-reconstruction.

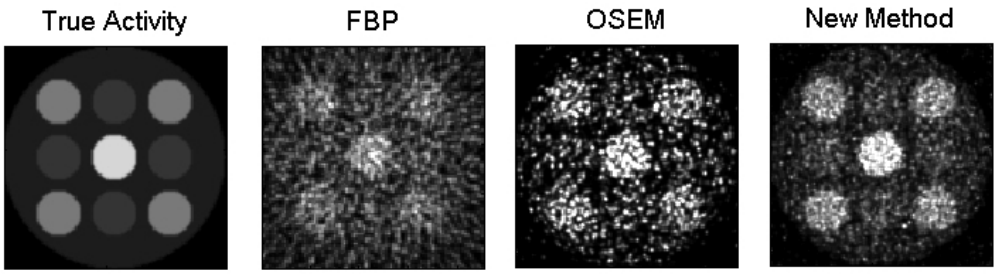

Figure 2. Example slices of the simulated 3D+t phantom: True activity image, FBP, OSEM and EMD (with non-stationary thresholding) methods. All images were post-reconstruction smoothed spatially using a 2D Gaussian with $\sigma = 0.7$voxels.

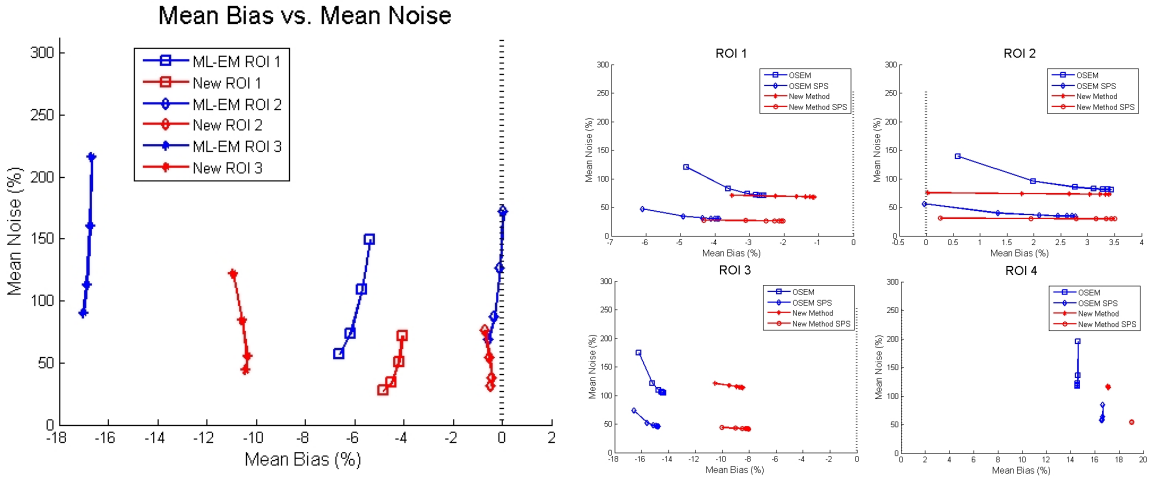

(a) Comparisons of different post-reconstruction spatial smoothing levels: $\sigma = 0, 0.5, 0.7, 0.9$(voxels).

(b) Comparisons of different post-reconstruction temporal smoothing levels (with and without post-reconstruction spatial smoothing (SPS)): $\sigma = 0.5, 1, 1.5, 2, 2.5, 3, 3.5$(timeframes).

Figure 3. Mean bias vs. mean noise for the conventional OSEM and our methods

3.3 Clinical 3D+t Colorectal PET Data

To aid validation of our EMD dynamic PET reconstruction technique we apply the algorithms to clinical colorectal data. A total of 321 million events where recorded for a 60 minute acquisition, obtained from Siemens Molecular Imaging. These events were then binned into twenty eight equal duration contiguous sinograms of size $336 \times 336 \times 313$. Results are again shown for the 64×64 central slice reconstruction.

Figure 4(a) shows the reconstructions of the final frame (128 seconds of data) for the EMD method with three levels of enhancement, FBP with and without post-Gaussian smoothing, and conventional OSEM with and without inter-iteration Gaussian smoothing. It appears that the EMD method significantly reduces noise due to the temporal regularisation, but without the need of user defined smoothing parameters. Figure 4(b) compares the TACs obtained by the various methods, demonstrating again that noise is reduced by the EMD method.

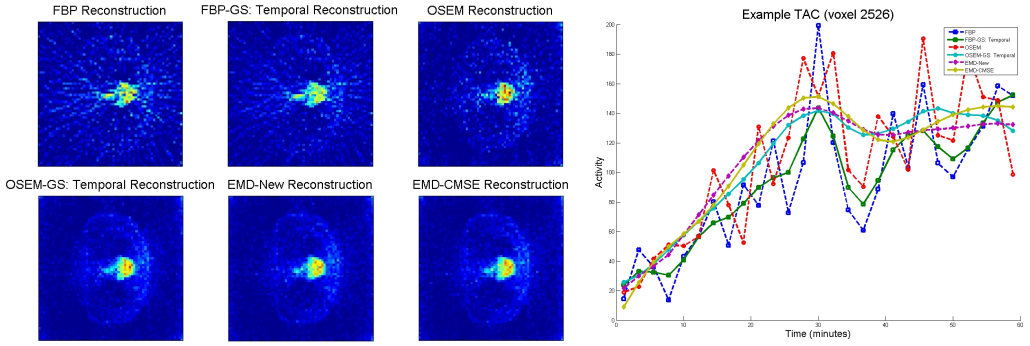

(a) Single central slice of frame 28 (b) Central voxel TACs

Figure 4. FBP, FBP with post-GS, OSEM, OSEM with inter-iteration GS, and EMD methods.

4 Conclusion

A novel dynamic PET reconstruction algorithm with temporal regularisation is proposed. The method ensures consistency between neighbouring frames using the EMD transform. Various EMD regularisation method are compared for both simulated and clinical dPET data and shown to lead to superior results than Gaussian smoothing. We note that if only pre-reconstructed dPET images are available, then a single application of our EMD denoising procedure will also improve the quality of the temporal images.

Acknowledgements

The authors would like to thank Anthonin Reilhac for the use of PET-SORTEO; Siemens Molecular Imaging for providing clinical data; and the Department for Business Enterprise and Regulatory Reform for their financial assistance.

References

1. B. Gundlich, P. Musmann & S. Weber. "Dynamic List-Mode Reconstruction of PET Data based on the ML-EM Algorithm." *IEEE Nuclear Science Symposium Conference Record* **5**, pp. 2791–2795, 2006.
2. T. Nichols et al. "Spatiotemporal Reconstruction of List Mode PET Data." *Trans.Med.Imag.* **23(4)**, pp. 396–404, 2002.
3. A. J. Reader, J. C. Matthews, F. C. Sureau et al. "Iterative Kinetic Parameter Estimation within Fully 4D PET Image Reconstruction." *IEEE Nuc. Sci. Symp. Conf.* **3**, pp. 1752–1756, 2006.
4. M. E. Kamasak, C. A. Bouman, E. D. Morris et al. "Direct Reconstruction of Kinetic Parameter Images from Dynamic PET Data." *IEEE Tran. Med. Imag.* **24(5)**, pp. 636–650, 2005.
5. R. Carson & K. Lange. "The EM Parametric Image Reconstruction Algorithm." *J. Am. Stat. Assoc.* **80**, pp. 20–22, 1985.
6. C. M. Kao, J. T. Yap, J. Mukherjee et al. "Image Reconstruction for Dynamic PET Based on Low-Order Approximation and Restoration of the Sinogram." *IEEE Transactions on Medical Imaging* **16(6)**, pp. 738–749, 1997.
7. M. N. Wernick, E. J. Infusino & M. Milosevic. "Fast Spatio-Temporal Image Reconstruction for Dynamic PET." *IEEE Trans. on Med. Imag.* **18(3)**, pp. 185–195, 1999.
8. M. Shidahara, Y. Ikoma, J. Kershaw et al. "PET Kinetic Analysis: Wavelet Denoising of Dynamic PET Data with Application to Parametric Imaging." *Ann Nucl Med* **21**, pp. 379–386, 2007.
9. N. Y. Lee & Y. Choi. "A Modified OSEM Algorithm for PET Reconstruction using Wavelet Processing." *Computer Methods and Programs in Biomedicine* **80(3)**, pp. 236–245, 2005.
10. J. Verhaeghe, D. V. Ville, I. Khalidov et al. "Dynamic PET Reconstruction Using Wavelet Regularization With Adapted Basis Functions." *MedImg* **27(7)**, pp. 943–959, 2008.
11. L. Shepp et al. "Maximum Likelihood Reconstruction for Emission Tomography." *Tran.Med.Imag.* **1(2)**, pp. 113–122, 1982.
12. B. W. Silverman, M. C. Jones, J. D. Wilson et al. "A smoothed em approach to indirect estimation problems, with particular reference to stereology and emission tomography." *Journal of the Royal Statistical Society. Series B* **52(2)**, pp. 271–324, 1990.
13. N. Huang & S. Shen. *Hilbert-Huang Transform and its Applications*. World Scientific Publishing Company, 2005.
14. S. Mallat. *A Wavelet Tour of Signal Processing, 2nd Edition (Wavelet Analysis & its Applications)*. Academic Press, 1999.
15. A. O. Boudraa, J. C. Cexus et al. "Noise Filtering Using Empirical Mode Decomposition." In *Inter. Symp. Sig. Proc. App.* 2007.
16. A. O. Boudraa et al. "EMD-Based Signal Noise Reduction." *International Journal of Signal Processing* **1**, pp. 33–37, 2004.
17. A. O. Boudraa & J. C. Cexus. "EMD-Based Signal Filtering." *IEEE Trans. Instr. Measur.* **56(6)**, pp. 2196–2202, 2007.
18. A. O. Boudraa & J. C. Cexus. "Denoising Via Empirical Mode Decomposition." In *Proc. IEEE ISCCSP*. 2006.
19. A. Reader, F. Sureau, C. Comtat et al. "Joint Estimation of Dynamic PET Images and Temporal Basis Functions using Fully 4D ML-EM." *Physics in Medicine and Biology* **51(21)**, pp. 5455–5474, 2006.
20. A. Reilhac, C. Lartizien et al. "PET-SORTEO: A Monte Carlo-based Simulator with High Count Rate Capabilities." *IEEE Trans. Nuc. Sci.* **51(1)**, pp. 46–52, 2004.